JBC RESEARCH ARTICLE

The long β2,3-sheets encoded by redundant sequences play an integral role in the channel function of P2X7 receptors

Received for publication, September 10, 2021, and in revised form, April 23, 2022 Published, Papers in Press, April 30, 2022,
https://doi.org/10.1016/j.jbc.2022.102002

Xue-Fei Ma[1,2,‡], Ting-Ting Wang[2,‡], Wen-Hui Wang[2,‡], Li Guan[2], Chang-Run Guo[2], Xing-Hua Li[2], Yun-Tao Lei[2], Ying-Zhe Fan[3], Xiao-Na Yang[2], Motoyuki Hattori[4], Osamu Nureki[5], Michael X. Zhu[6], Ye Yu (于烨)[2,*], Yun Tian (田云)[1,*], and Jin Wang (汪津)[2,*]

From the [1]College of Bioscience and Biotechnology, Hunan Agricultural University, Changsha, China; [2]School of Basic Medicine and Clinical Pharmacy and State Key Laboratory of Natural Medicines, China Pharmaceutical University, Nanjing, China; [3]Putuo Hospital, Shanghai University of Traditional Chinese Medicine, Shanghai, China; [4]State Key Laboratory of Genetic Engineering, Collaborative Innovation Center of Genetics and Development, Shanghai Key Laboratory of Bioactive Small Molecules, Department of Physiology and Neurobiology, School of Life Sciences, Fudan University, Shanghai, China; [5]Department of Biological Sciences, Graduate School of Science, The University of Tokyo, Bunkyo-ku, Tokyo, Japan; [6]Department of Integrative Biology and Pharmacology, McGovern Medical School, The University of Texas Health Science Center at Houston, Houston, Texas, USA

Edited by Mike Shipston

P2X receptors are a class of nonselective cation channels widely distributed in the immune and nervous systems, and their dysfunction is a significant cause of tumors, inflammation, leukemia, and immune diseases. P2X7 is a unique member of the P2X receptor family with many properties that differ from other subtypes in terms of primary sequence, the architecture of N- and C-terminals, and channel function. Here, we suggest that the observed lengthened β2- and β3-sheets and their linker (loop β2,3), encoded by redundant sequences, play an indispensable role in the activation of the P2X7 receptor. We show that deletion of this longer structural element leads to the loss of P2X7 function. Furthermore, by combining mutagenesis, chimera construction, surface expression, and protein stability analysis, we found that the deletion of the longer β2,3-loop affects P2X7 surface expression but, more importantly, that this loop affects channel gating of P2X7. We propose that the longer β2,3-sheets may have a negative regulatory effect on a loop on the head domain and on the structural element formed by E171 and its surrounding regions. Understanding the role of the unique structure of the P2X7 receptor in the gating process will aid in the development of selective drugs targeting this subtype.

P2X receptors are ligand-gated nonselective cation channels activated by extracellular ATP (1, 2). To date, seven subtypes of the P2X receptor family have been identified as P2X1-P2X7 (1, 3–7). Among them, P2X7 has many features that differ from other P2X subtypes, such as the fact that P2X7 requires very high concentrations of ATP for activation and has an EC_{50} value (the concentration that produces half of the maximal response) of approximately 0.3 to 1 mM under normal physiological conditions (2 mM extracellular Ca^{2+} and 1 mM extracellular Mg^{2+}), whereas the EC_{50} values of other subtypes are generally around 0.5 to 10 μM (8). In terms of the channel desensitization of P2X receptors, P2X1 and P2X3 desensitize very quickly (milliseconds) after saturating ATP applications, whereas P2X2 and P2X4 are relatively slow (seconds); P2X7 does not desensitize at all (9, 10), even though prolonged activation leads to pore dilation of P2X7, allowing permeation of small molecules with molecular weights up to 900 Da (11, 12). The aforementioned unique properties make P2X7 considered as the most special member of the P2X family compared to other subtypes.

P2X7 receptors are involved in many physiopathological functions, particularly its expression in lymphocytes, macrophages, and microglia, and its role in the immune response (13). It has been shown that P2X7 receptors are required for the establishment of long-lived memory $CD8^+$ cells (14). P2X7 receptors are expressed in neutrophils, and their activation leads to activation of nod-like receptor family pyrin domain-containing 3 inflammasome and secretion of interleukin-1β (IL-1β) (15), indicating that P2X7 receptors are closely associated with inflammation. P2X7 plays a role in allograft transplant rejection, and inhibition of the P2X7 receptor or the nod-like receptor family pyrin domain-containing 3 inflammasome contributes to the induction of graft tolerance (16). P2X7 in the central nervous system is involved in the neurodegenerative diseases, such as Alzheimer's disease (17), Huntington's disease (18), and multiple sclerosis (19). In addition, P2X7 receptors are inextricably linked to cancer (20) and pain (21). Therefore, P2X7 receptors are one of the important new drug targets in recent years (22–24).

The gating mechanism based on the structure of each P2X receptor subtype has been well studied. The first crystal structure of the zebrafish P2X4 (zfP2X4) receptor was determined in 2009 (25), and the structures of several other P2X subtypes have been determined in the last decade (26–32). The

‡ These authors contributed equally to this work.
* For correspondence: Jin Wang, wangjin@cpu.edu.cn; Yun Tian, tianyun79616@163.com; Ye Yu, yuye@cpu.edu.cn.

overall three-dimensional (3D) structure of the P2X receptor and the way that each subunit is folded are essentially the same for all subtypes: each P2X subtype exhibits a "chalice"-like trimeric structure containing a large hydrophilic extracellular structural domain, two transmembrane helices and intracellular termini, and the individual subunits of each P2X subtype resemble “dolphins”. Nevertheless, the gating differences between P2X subtypes are not fully understood, especially the unique P2X7 receptor. In addition to its function and properties being specific among P2X subtypes, the structure of P2X7 is unique, starting with the long intracellular N- and C-terminals of P2X7. The C-terminus of P2X7 is involved in regulating many functions of the P2X7 receptor, including protein–protein interactions, phosphorylation, and post-translational modifications (33). In contrast to other P2X receptors, the C-terminus of P2X7 has a unique cysteine-rich region called the "C-cys anchor" that prevents P2X7 receptor desensitization (30, 34), and approximately 20 amino acid residues at the C-terminus form a unique structure called the “cytoplasmic ballast”. The N-terminal of P2X7 is important for Ca^{2+}-influx (35), channel activation facilitation (34), and the activation of extracellular signal–regulated kinases (36). In addition, despite binding the U-shape of ATP and key residues recognized by ATP (K64, K66, T189, N292, R294 and K311, rP2X7 numbering) are conserved in the P2X receptor family, but recent structures have shown that the ATP-binding pocket of the P2X7 receptor is narrower than that of the human P2X3 (hP2X3) receptor (29, 30). Thus, P2X7 is structurally unique in many ways compared to other subtypes, and all of these unique structural elements are associated with functions that distinguish it from other subtypes.

Here, we find another unique structural element of P2X7. By comparison of structure and sequence, we found that the β2 and β3 sheets of P2X7 and their linker (loop β2,3) are longer compared to other subtypes. The question of whether the longer β2,3-sheet and loop β2,3 of the P2X7 receptor have a unique function compared to other P2X receptor subtypes remains unclear. In this study, we show that the redundant sequence between the P2X7 receptor β2,3 and its corresponding structural elements plays an important role in both expression and channel gating of the P2X7 receptor, which is unique among the P2X family.

Results

P2X7 receptors have a longer β2,3-sheet that is necessary for channel activation

Sequence alignment analysis of the P2X receptor family revealed that residues 73 to 80 of the P2X7 receptor are redundant compared to other subtypes (Fig. 1*C*). In the recently determined resting-state structure of rP2X7 (PDB ID: 6U9V), no stable conformation of this region was observed in this disordered region; however, in the open state, this region folded into a longer β2,3 in the cryo-electron microscopic (Cryo-EM) structure of the P2X7 receptor than that of the P2X3 receptor (Fig. 1, *A* and *B* and PDB IDs: 6U9W and 5SVK). The superposition of the resting and open states showed that the longer β2,3 region shifted to the right in the open state (Fig. 1, *A* and *B*).

To verify whether the longer β2,3 structure in the P2X7 receptor is necessary for channel function, we deleted residues 73 to 80 and obtained Δ(73–80). Δ(73–80) mutant significantly reduced the 1 mM ATP-induced currents (70.9 ± 57.8 and 250 ± 61 pA/pF, for Δ(73–80) and wildtype, WT, n = 4 and 13, respectively, $p < 0.01$, Δ(73–80) *versus* WT; Fig. 2, *A* and *B*). We also performed a smaller deletion of this fragment and obtained three truncations, Δ(73–74), Δ(75–76), and Δ(77–80), where Δ(73–74) dramatically decreased the function of the channel. However, mutations in N73A and N74A at individual positions did not have as strong an effect as that caused by deleting both of them (Fig. 2, *A* and *B*). Moreover, the EC_{50} values of Δ(73–80) (208.7 ± 22.6 μM), Δ(73–74) (1762.3 ± 5.8 μM), Δ(75–76) (335.4 ± 88.2 μM), E73A (33.9 ± 1.7 μM), and N74A (26.6 ± 0.2 μM) were significantly changed compared to rP2X7 WT (98.5 ± 37.3 μM) (Fig. 2*C*). These results suggest that this redundant structure may not facilitate

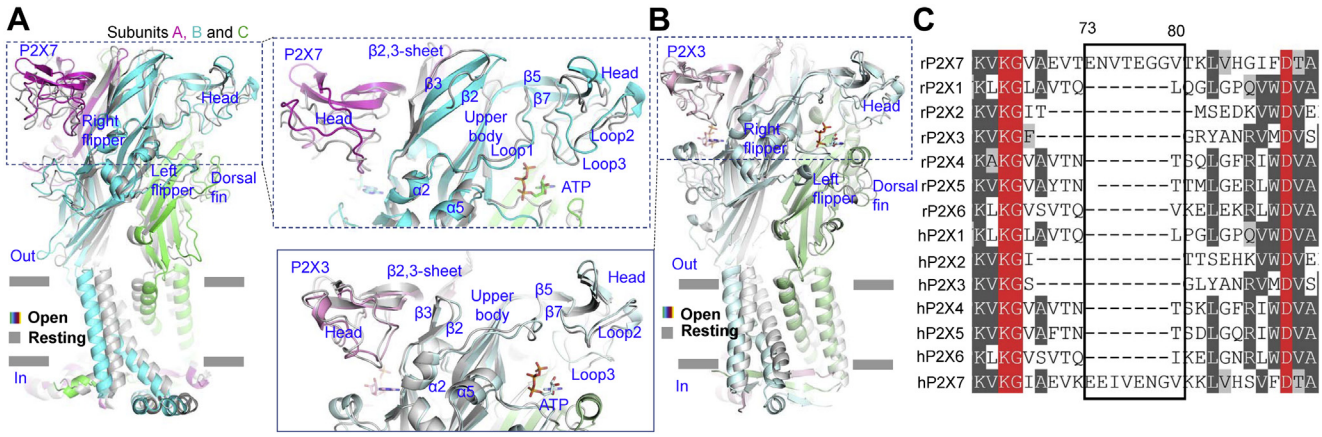

Figure 1. The β2,3-sheet of P2X7 receptor is longer than other subtypes. *A* and *B*, a superposition of resting (*gray*) and open (*color*) conformations of rP2X7 (PDB IDs: 6U9W and 6U9V for resting and open states, respectively, *A*) and hP2X3 (PDB IDs: 5SVJ and 5SVK for resting and open states, respectively, *B*). The *dashed box* highlights the β2,3-sheet and its surrounding regions. *C*, sequence alignment of the P2X receptor family. *Black boxes* represent redundant sequences encoding longer β2,3-sheet.

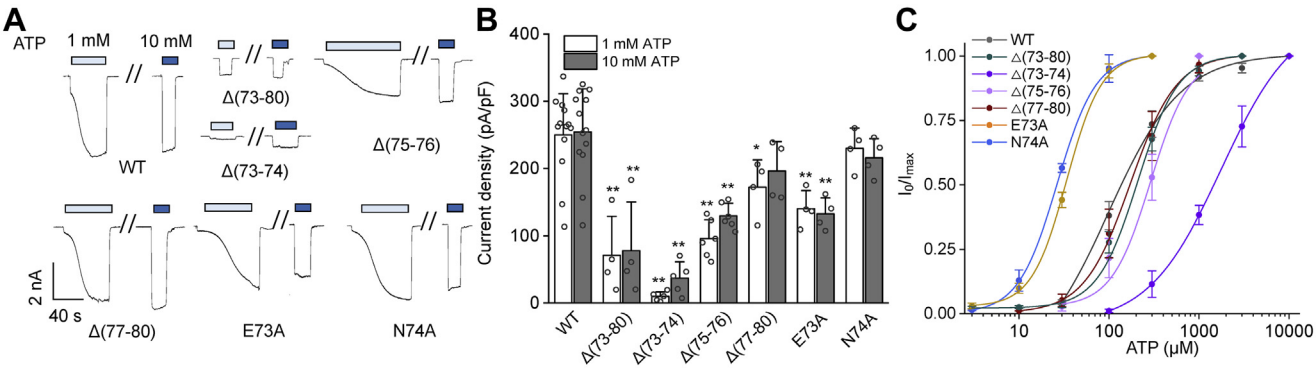

Figure 2. Deletion of the redundant region 73 to 80 affects the channel function of the rP2X7 receptor. *A* and *B*, representation current traces (*A*) and pooled data (*B*) for wildtype (WT) and mutants of rP2X7. The scatter of each open circle represents each measurement (mean ± S.D., n = 4–13). $^{**}p < 0.01$, $^{*}p < 0.05$ *versus* WT, two-way ANOVA with Bonferroni post hoc test ($F(6, 66) = 39.56$, $p < 0.0001$). *C*, dose–response curves of ATP in WT and mutated rP2X7 receptors. *Solid lines* were fitted by the Hill1 equation (mean ± S.E.M., n = 4–7).

interactions with surrounding residues through individual amino acids but rather participate in channel gating together as an integrated whole.

In addition to gating modulation, there are many factors that can affect the maximum current of a channel. First, we analyzed the membrane expression of these mutants. We found that Δ(73–80), Δ(73–74), Δ(75–76), and Δ(77–80) had significantly reduced numbers of membrane proteins (Fig. 3, *A* and *B*), which suggests that the reduction in the maximum currents of Δ(73–80), Δ(73–74), and Δ(75–76) channels may be caused by the reduction in surface expression of channels. However, there was no significant difference in the surface expression of these mutants, such as Δ(73–74), whose maximum current density was significantly reduced, but whose membrane expression was the same as that of E73A and N74A (maximum current density of E73A and N74A was only slightly lower or not different from that of WT, Fig. 2, *A* and *B*). In addition, the surface/total ratio was also calculated (Fig. 3*C*) and correlation analysis showed no correlation between surface/total ratio and current density ($R^2 = 0.48$, $p = 0.08$, Pearson's correlation, Fig. 3*D*). These results indicate that some reduction in membrane expression did not contribute mainly to the reduction in the maximum current density of the mutants.

In addition, we treated cells transfected with rP2X7 WT and Δ(73–80) with cyclohexanone (20 μg/ml) for different times to see if there was an effect on protein stability. Even after 10 h of cyclohexanone treatment, the amount of protein was not affected (Fig. 3, *E* and *F*). Once factors of protein surface expression and stability were excluded, we inferred that the reduction in the maximum current may be caused by gating changes in the channel due to the lack of the longer β2,3 structure of P2X7.

E171, a residue near the β2,3-sheet, has an important role in channel activation that differs from that of other subtypes

The β2,3-sheet in the structure of each P2X receptor is sandwiched between the upper body domain of the same subunit and the head domain of the adjacent subunit (Fig. 1, *A* and *B*). In addition, the conformation of the β2,3-sheet of rP2X7 changed considerably from the resting state to the open state. In the resting state, the exact conformation cannot be seen due to insufficient resolution, but it should not be a stable β-sheet (30). Therefore, residues 73 to 80 of rP2X7 may have a loose loop-like secondary structure in the resting state, while in the open state, they form a rigid β-sheet (Fig. 1*A*). Notably, the longer region (residues 73–80) of the β2,3-sheet in P2X7 is closer to the upper body domain of the same subunit than that of other subtypes (Fig. 1, *A* and *B*). The superposition of the resting and open state structures of rP2X7 revealed that the conformation of the loop 168 to 175 (loop 1) in the upper body domain of the same subunit changed significantly, while the longer β2,3 shifted to the right, as evidenced by the apparent flip-flopping of the side chains of amino acids A170, E171, and E172 (Fig. 4*A*).

We further mutated each of these three amino acids and found that mutation of E171A significantly reduced the function of the channel (3.5 ± 1.4 and 314 ± 79 pA/pF for E171A and WT, respectively, $p < 0.01$, E171A *versus* WT; Fig. 4, *B* and *C*) even when the concentration of ATP was increased to 30 mM and it did not further increase the current density (2.1 ± 1.5 pA/pF for E171A, saturated ATP). E171D, a mutation with more similar side chain properties, still significantly impaired channel activation of rP2X7, suggesting a rigid requirement of this position for rP2X7 activation (112 ± 42, 151 ± 60, and 173 ± 62 pA/pF after the treatment of 1, 10, and 30 mM ATP, respectively, in E171D; Fig. 4*D*). E171D significantly changed the apparent ATP affinity of rP2X7 (EC_{50} = 127 ± 41 and 752 ± 18 μM for rP2X7 WT and E171D, respectively; Fig. 4*E*). In addition, Western blot experiments showed that E171A did not cause abnormal surface expression of rP2X7 (Fig. 4, *F* and *G*). These results suggest that residue E171 in the region adjacent to the longer β2,3 region (residues 73–80) is also critical for the gating process of P2X7.

Does E171, like the longer β2,3 redundant region, has a unique effect on the maximum current of rP2X7 compared to other members of the P2X family? To explore this idea, we performed a sequence alignment analysis and found that E171 is highly conserved in the P2X family (Fig. 5*A*). Therefore, we

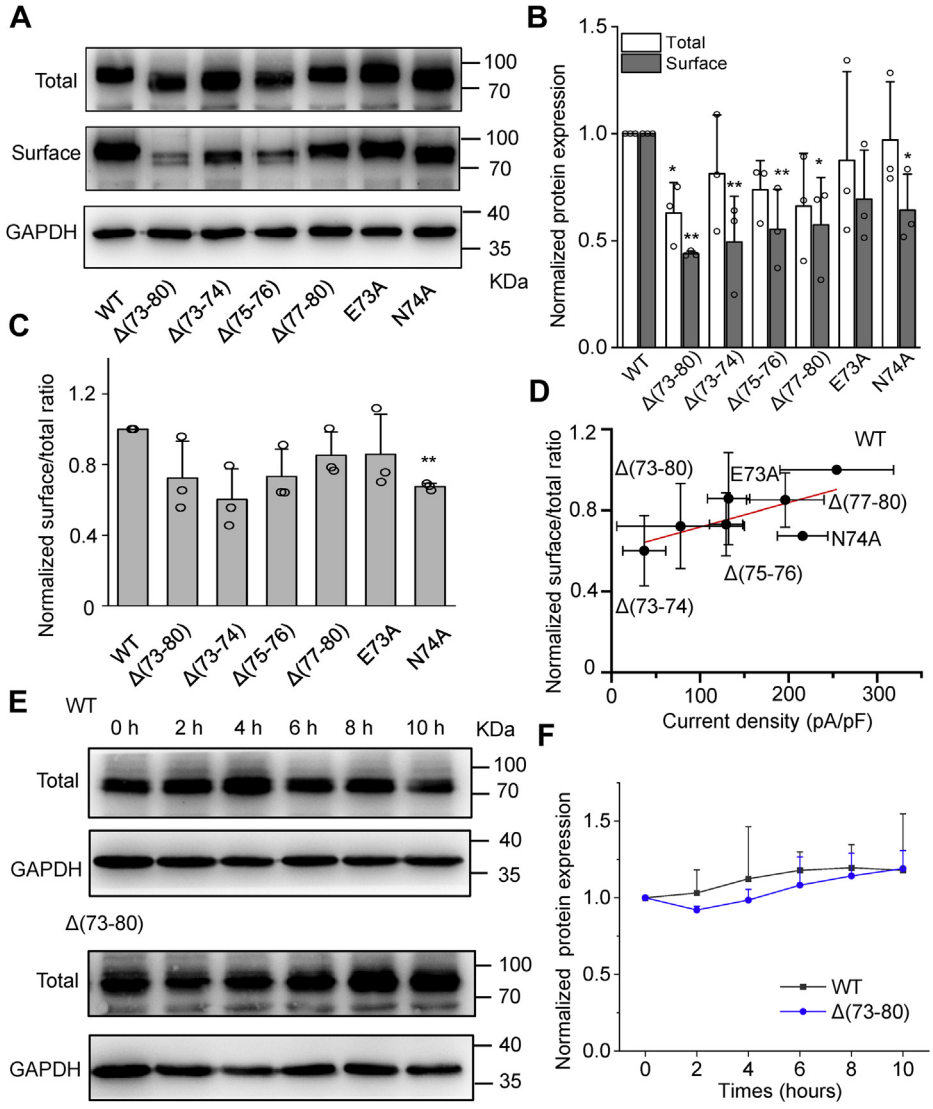

Figure 3. Deletion of the redundant region 73 to 80 affects P2X7 channel expression but not protein stability. *A* and *B*, representative Western blotting (*A*) and pooled data (*B*) of total and surface protein expressions of rPX7 WT and mutant channels. Data are expressed as mean ± S.D. (n = 3) at total or surface level, normalized to WT protein, $^{**}p < 0.01$, $^{*}p < 0.05$ compared to WT, two-way ANOVA with Bonferroni post hoc test ($F(6,24) = 6.459$, $p = 0.0004$). *C*, normalized surface/total ratio of rP2X7 WT and mutant channels (mean ± S.D., n = 3), normalized to WT protein; $^{**}p < 0.01$ compared to WT, one-way ANOVA with Bonferroni post hoc test ($F(2, 12) = 1.074$, $p = 0.3724$). *D*, correlation between surface/total ratio and the current density ($R^2 = 0.48$, $p = 0.08$, Pearson's correlation). *E*, representative Western blot analysis of total and surface expressions of rP2X7 WT and Δ(73–80) mutant. HEK-293 cells expressing WT or Δ(73–80) were treated with 20 μg/ml CHX, and time-series experiments were performed as indicated. Results were observed in at least three independent experiments for statistical analysis. *F*, time response curves (mean ± S.D., n = 3) showing protein expression levels at different time points after incubation with 20 μg/ml CHX.

performed the same point mutation in the identical position for other P2X subtypes. There are no or only small ATP-induced currents in the P2X5 and P2X6 subtypes, and thus, no mutations were made to these two subtypes. In P2X1 to P2X4, mutations at this position resulted in significant changes (~10-fold) in the EC_{50} values of P2X1, P2X3, and P2X4 (EC_{50} = 0.67 ± 0.03 and 4.39 ± 0.84 μM for P2X1 WT and E168A, respectively; 0.48 ± 0.31 and 0.64 ± 0.24 μM for P2X3 WT and E156A, respectively; 7.04 ± 4.41 and 52.0 ± 18.6 μM for P2X4 WT and E168A, respectively; Fig. 5, *B*, *F* and *H*). For the P2X2 subtype, mutation E167A did not affect the EC_{50} of ATP (EC_{50} = 24.0 ± 7.8 and 27.5 ± 3.9 μM for P2X2 WT and E167A, respectively; Fig. 5*D*). Unlike P2X7, none of the mutations in these subtypes altered the maximum current density of ATP (Fig. 5, *C*, *E*, *G* and *I*), suggesting that E171 of rP2X7 plays a different role in channel function than other subtypes, at least for P2X1-4.

The longer β2,3-sheet and the linker, loop β2,3, are functionally interconnected with E171 in the P2X7 receptor

Although both β2,3 and E171 in rP2X7 affect channel gating and both are specific to the P2X7 subtype, whether the two are interrelated needs further verification. To address this issue, we explored the effects of these two regions of P2X7 on channels in different species, including human P2X7 (hP2X7), panda P2X7 (pdP2X7), dog (dP2X7), guinea pig P2X7 (gpP2X7), mouse P2X7 (mP2X7), bovine P2X7 (bP2X7), and chicken P2X7

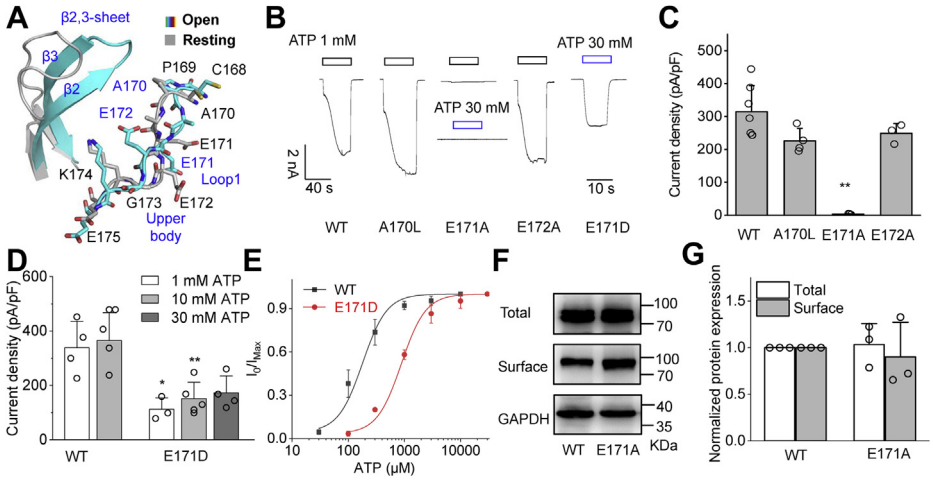

Figure 4. E171 in the loop one of the upper body domain is essential for channel gating of the P2X7 receptor. *A*, superimposition of the resting (*gray*) and open (*blue*) states of rP2X7, showing the motion of loop 1 (in the *upper domain*) and the β2,3-sheet. *B* and *C*, representative current traces (*B*) and pooled data (*C*) for WT and E171A. Data are expressed as mean ± S.D. (n = 4–6), $^{**}p < 0.01$, one-way ANOVA with Bonferroni post hoc test ($F(3, 13) = 20.42$, $p < 0.0001$). *D*, summary of current densities for rP2X7 WT and E171D induced by 1 mM ATP (*white*), 10 mM ATP (*light gray*), and 30 mM ATP (*dark gray*). Data are expressed as mean ± S.D. (n = 4–5), $^{*}p < 0.05$ and $^{**}p < 0.01$ *versus* WT. Student's *t* test, $p = 0.0139$ (1 mM ATP) and $p = 0.00568$ (10 mM ATP). *E*, concentration response curves of ATP in rP2X7 WT and E171D. *Solid lines* were fitted by the Hill1 equation (mean ± S.D., n = 3). *F* and *G*, representative Western blots (*F*) and pooled data (*G*) of the total and surface protein expression of rP2X7 WT and E171A (mean ± S.D., n = 3).

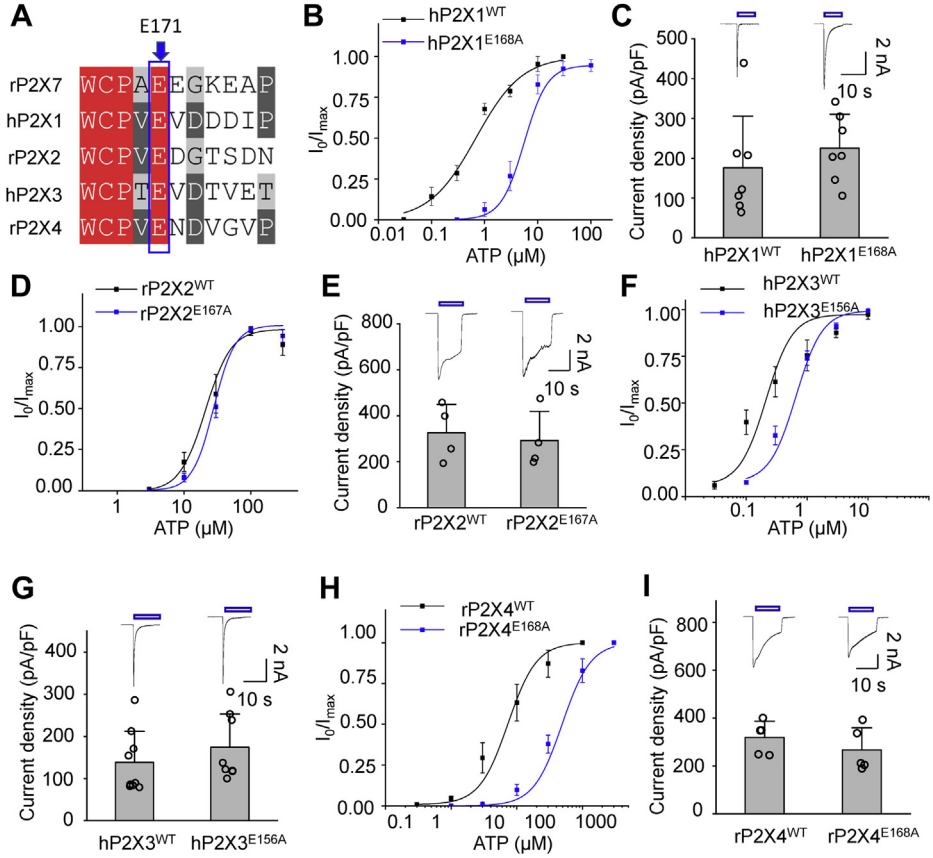

Figure 5. Role of residues at the same position as E171 in other P2X subtypes. *A*, sequence alignment of the E171 position in the P2X receptor family (P2X1-7). The *blue boxed* region highlights residue E171 (rP2X7 numbering), which is conserved in the P2X family. *B–I*, concentration response curves for ATP, representative current traces and pooled data for hP2X1 (*B* and *C*), rP2X2 (*D* and *E*), hP2X3 (*F* and *G*), rP2X4 (*H* and *I*) and their mutants. The *solid lines* are fitted by Hill1 equation (mean ± S.D., $EC_{50} = 0.67 \pm 0.03$ and 4.39 ± 0.84 μM for $hP2X1^{WT}$ and $hP2X1^{E168A}$, respectively, n = 3–4; $EC_{50} = 24.01 \pm 7.83$ and 27.50 ± 3.89 μM for $rP2X2^{WT}$ and $rP2X2^{E167A}$, respectively, n = 4; $EC_{50} = 0.48 \pm 0.31$ and 0.64 ± 0.24 μM for $hP2X3^{WT}$ and $hP2X3^{E156A}$, respectively, n = 3–4; $EC_{50} = 7.04 \pm 4.41$ and 52.0 ± 18.6 μM for $rP2X4^{WT}$ and $rP2X4^{E168A}$, respectively, n = 3–4).

(ckP2X7). In these genes, ckP2X7 has a different sequence, i.e., it does not have a longer β2,3-sheet like other P2X7, and the identical E171 position is Q159 (Fig. 6*A*). As expected, the mutant ckP2X7^{Q159A} does not affect the maximum current of this channel (353 ± 121 and 387 ± 164 pA/pF for ckP2X7^{Q159A} and ckP2X7^{WT}, respectively; $p > 0.05$, ckP2X7^{Q159A} *versus* ckP2X7^{WT}; Fig. 6, *B* and *C*). Since other species have the longer β2,3 and a conserved glutamate at the same position as 171, we deleted the redundant region of β2,3 and mutated residues at the corresponding positions of E171 in these species to obtain pdP2X7$^{Δ(73-80)}$, pdP2X7^{E171A}, hP2X7$^{Δ(73-80)}$, hP2X7^{E171A}, dP2X7$^{Δ(73-80)}$, dP2X7^{E171A}, gpP2X7$^{Δ(73-80)}$, gpP2X7^{E171A}, mP2X7$^{Δ(73-80)}$, mP2X7^{E171A}, bP2X7$^{Δ(75-82)}$, and bP2X7^{E173A}.

Removing the redundant sequence, pdP2X7$^{Δ(73-80)}$, does not affect the maximum current of this channel, and therefore, the mutation in pdP2X7^{E171A} does not affect the maximum current either (325 ± 55 and 260 ± 59 pA/pF for pdP2X7^{E171A} and pdP2X7^{WT}, respectively; pdP2X7^{E171A} *versus* pdP2X7^{WT}, $p > 0.05$; Fig. 6, *D* and *E*). As well, the surface/total expression ratios of pdP2X7$^{Δ(73-80)}$ and pdP2X7^{E171A} were comparable to that of pdP2X7^{WT}(Fig. 7, *A*–*C*). In contrast, deletions corresponding to rP2X7 are similar in the other five species: mutations corresponding to the β2,3 redundant region and E171 position both significantly affect the maximum current of the P2X7 channel in these species (28.3 ± 10.7, 3.5 ± 2.6, and 74.9 ± 35.4 pA/pF for hP2X7$^{Δ(73-80)}$, hP2X7^{E171A}, and hP2X7^{WT}, respectively, $p < 0.01$, n = 11, 7, and 7, Fig. 6, *F* and *G*; 73.1 ± 52.7, 65.0 ± 36.7, and 222 ± 72 pA/pF for dP2X7$^{Δ(73-80)}$, dP2X7^{E171A}, and dP2X7^{WT}, respectively, $p < 0.01$, n = 6, 4, and 5, Fig. 6, *H* and *I*; 0.54 ± 0.54, 41.3 ± 28.5, and 356 ± 100 pA/pF for gpP2X7$^{Δ(73-80)}$, gpP2X7^{E171A}, and gpP2X7^{WT}, respectively, $p < 0.01$, n = 3, 4, and 3, Fig. 6, *J* and *K*; 91.3 ± 20.5, 5.8 ± 3.4, and 146 ± 12 pA/pF for mP2X7$^{Δ(73-80)}$, mP2X7^{E171A}, and mP2X7^{WT}, respectively, $p < 0.05$, n = 4, 4, and 4, Fig. 6, *L* and *M*; 1.5 ± 1.7, 4.4 ± 3.2, and 185 ± 53 pA/pF for bP2X7$^{Δ(75-82)}$, bP2X7^{E173A}, and bP2X7^{WT}, respectively, $p < 0.01$, n = 4, 3, and 3, Fig. 6, *N* and *O*).

In addition, we examined the membrane expression-to-total expression ratios of other three different species of P2X7 (dP2X7, mP2X7, and bP2X7) and their corresponding mutants (dP2X7$^{Δ(73-80)}$, mP2X7$^{Δ(73-80)}$, and bP2X7$^{Δ(75-82)}$) by Western blot. dP2X7$^{Δ(73-80)}$ membrane expression was somewhat

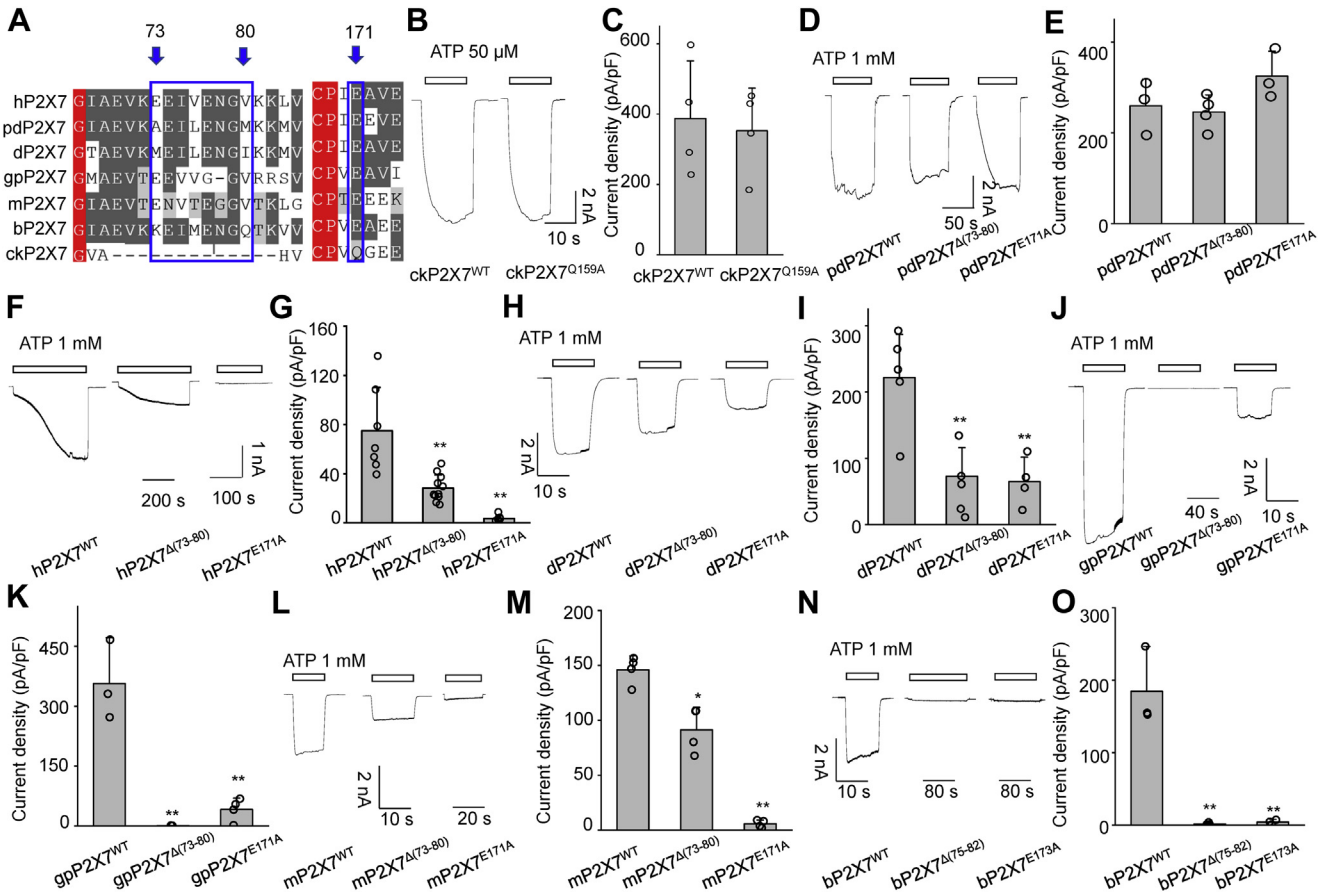

Figure 6. Effects of 73 to 80 and E171 in P2X7 receptors from different species. *A*, sequence alignment of P2X7 receptors from different species at positions 171 and 73 to 80 are highlighted in the boxed area. *B*–*O*, representative current traces and pooled data of WT and alanine substitutions for P2X7 receptors of different species at equivalent positions: ckP2X7 (chicken P2X7) (*B* and *C*), pdP2X7 (panda P2X7) (*D* and *E*), hP2X7 (human P2X7) (*F* and *G*), dP2X7 (dog P2X7) (*H* and *I*), gpP2X7 (guinea pig P2X7) (*J* and *K*), mP2X7 (mouse P2X7) (*L* and *M*), and bP2X7 (bovine P2X7) (*N* and *O*). Data were presented as mean ± S.D. (n = 3–13), $^{**}p < 0.01$, $^{*}p < 0.05$ *versus* WT, student's *t* test, $p > 0.05$ for ckP2X7, one-way ANOVA with Bonferroni post hoc test $F(2, 7) = 2.38$, $p = 0.1627$ for pdP2X7; $F(2, 22) = 23.54$, $p < 0.0001$ for hP2X7; $F(2, 12) = 11.87$, $p = 0.0014$ for dP2X7; $F(2, 7) = 36.95$, $p = 0.0002$ for gpP2X7; $F(2, 9) = 100.5$, $p < 0.0001$ for mP2X7; and $F(2, 7) = 42.24$, $p = 0.0001$ for bP2X7.

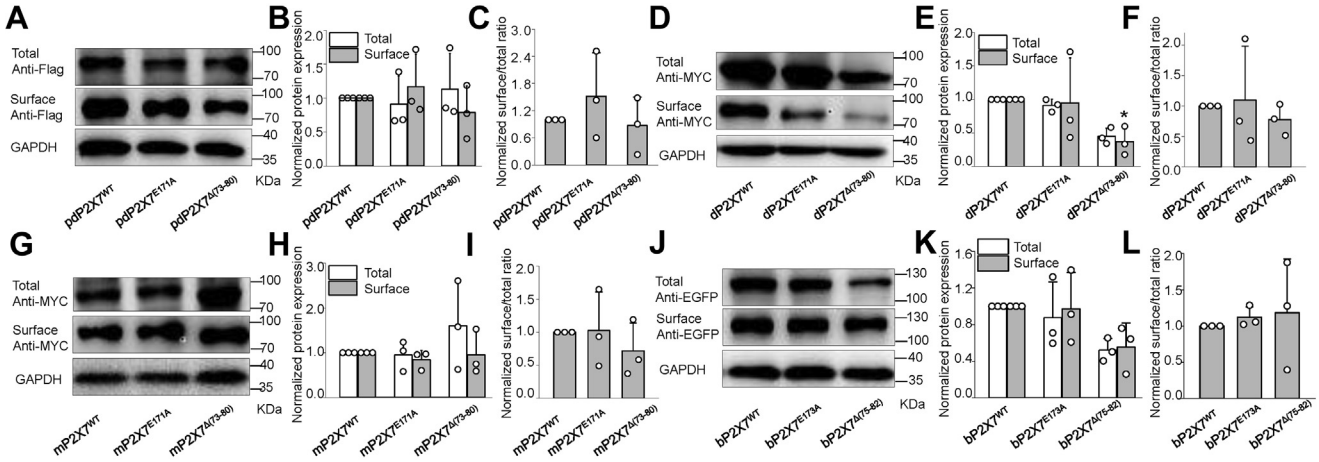

Figure 7. Western blot analysis of the total and surface expression of P2X7 WT and mutant channels of different species. *A–C*, representative Western blotting (*A*), pooled data of total and surface protein expressions (*B*), and surface/total ratio (*C*) of pdP2X7 WT and mutant channels (mean ± S.D., n = 3). Anti-Flag antibody was used to detect the expression of pdP2X7. *D–F*, representative Western blotting (*D*), pooled data of total and surface protein expressions (*E*), and surface/total ratios (*F*) of dP2X7 WT and mutant channels (mean ± S.D., n = 3). Anti-MYC antibody was used to detect the expression of dP2X7. *$p < 0.05$ *versus* WT, two-way ANOVA with Bonferroni post hoc test ($F(2,8) = 9.440$, $p = 0.0078$). *G–I*, representative Western blotting (*G*), pooled data of total and surface protein expressions (*H*), and surface/total ratio (*I*) of mP2X7 WT and mutant channels (mean ± S.D., n = 3). Anti-MYC antibody was used to detect the expression of mP2X7. *J–L*, representative Western blotting (*J*), pooled data of total and surface protein expressions (*K*), and surface/total ratios (*L*) of bP2X7 WT and mutant channels (mean ± S.D., n = 3). Anti-GFP antibody was used to detect the expression of bP2X7.

decreased compared to WT (Fig. 7, *D–F*). However, there was no significant difference between $mP2X7^{\Delta(73\text{-}80)}$ and $bP2X7^{\Delta(75\text{-}82)}$ and WT (Fig. 7, *G–L*). These results suggest that the deletion of the longer β2,3 in P2X7 causes a decrease in membrane expression (as in rP2X7) that varies among species.

Based on the aforementioned results, there is a relationship between these two structural elements, i.e., when the redundant region influences the maximum current, the E171 position also has an effect; when there is no redundant region or the redundant region has no effect on the maximum current, then the E171 also has no effect. Moreover, this linkage does not appear to be strongly associated with redundant regions affecting protein membrane expression or not.

The longer β2,3-sheet of the P2X7 receptor negatively regulates P2X7 activation in combination with loop structures near E171

Next, we investigated the mechanism of the interrelationship between the β2,3 redundant region and E171. Since the β2,3 redundant region/E171 of pdP2X7 and rP2X7 have a diametrically opposed role in the channel activation and the crystal or cryo-EM structures of both have been determined, we used both species of P2X7 for the following studies. rP2X7 structural superposition in the resting and open states showed that hydrogen bonding interactions were formed between R294 and E171 in both the resting and open states, except that in the resting state R294....E171 salt bridge is positioned further away from the ATP-binding site than in the open state (Fig. 8*A*). In this process, ATP attracts R294, prompting E171 to move and its side chain orientation to change, resulting in the R294...E171 salt bridge as a whole toward the ATP-binding site, further leading to the aforementioned conformational flip of E171 in the loop 1 (residues 168–175, rP2X7 numbering) (Fig. 8*A*). In addition, the head domain movement of the P2X7 receptor is upward upon ATP binding, and there is a clear positional shift in a segment of the loop structure in the head domain (which we call loop 2, residues 121–139, rP2X7 numbering), in contrast to that of other subtypes. Interestingly, in the *apo* structure of the pdP2X7 receptor, the position of E171 and the conformation of loop 2 are similar to the open structure of rP2X7, but different from that of the resting state (Fig. 8*B*). The difference led us to speculate that the redundant β2,3 structure could facilitate the conformational transition from the resting to the open state of E171 and surrounding structural elements in the rP2X7 receptor and that the differences between rat and panda species may be caused by sequence differences in the β2,3-sheet.

Therefore, we replaced the β2,3 region of rP2X7 with the corresponding region of pdP2X7 to construct $rP2X7^{CH1}$ (Fig. 8*C*). Such a replacement resulted in a certain reduction in the maximum channel current (82.9 ± 35.4 and 204 ± 57 pA/pF for $rP2X7^{CH1}$ and $rP2X7^{WT}$, respectively, $p < 0.01$, $rP2X7^{CH1}$ *versus* $rP2X7^{WT}$, n = 7 and 6; Fig. 8, *D* and *E*). On this basis, E171A was mutated to obtain $rP2X7^{CH1/E171A}$. The result was not the unaltered current we expected but rather a complete loss of function. $rP2X7^{\Delta(73\text{-}80)/E171A}$, the mutant E171A based on Δ(73–80), also had an almost negligible ATP response. These results suggest that it is not only the sequence of the β2,3 region that determines the interrelationship between β2,3 and E171.

The structural difference between rP2X7 and pdP2X7 not only lies in the position of E171 but may also include the region of loop 2 (121–139). To test the role of loop 2 in the difference between rP2X7 and pdP2X7, we first replaced loop 2 of rP2X7 with pdP2X7 to obtain $rP2X7^{CH2}$ (Fig. 8*F*); this replacement did not affect the function of the channel (Fig. 8, *G* and *H*). Then, mutating E171A on top of this chimera, we

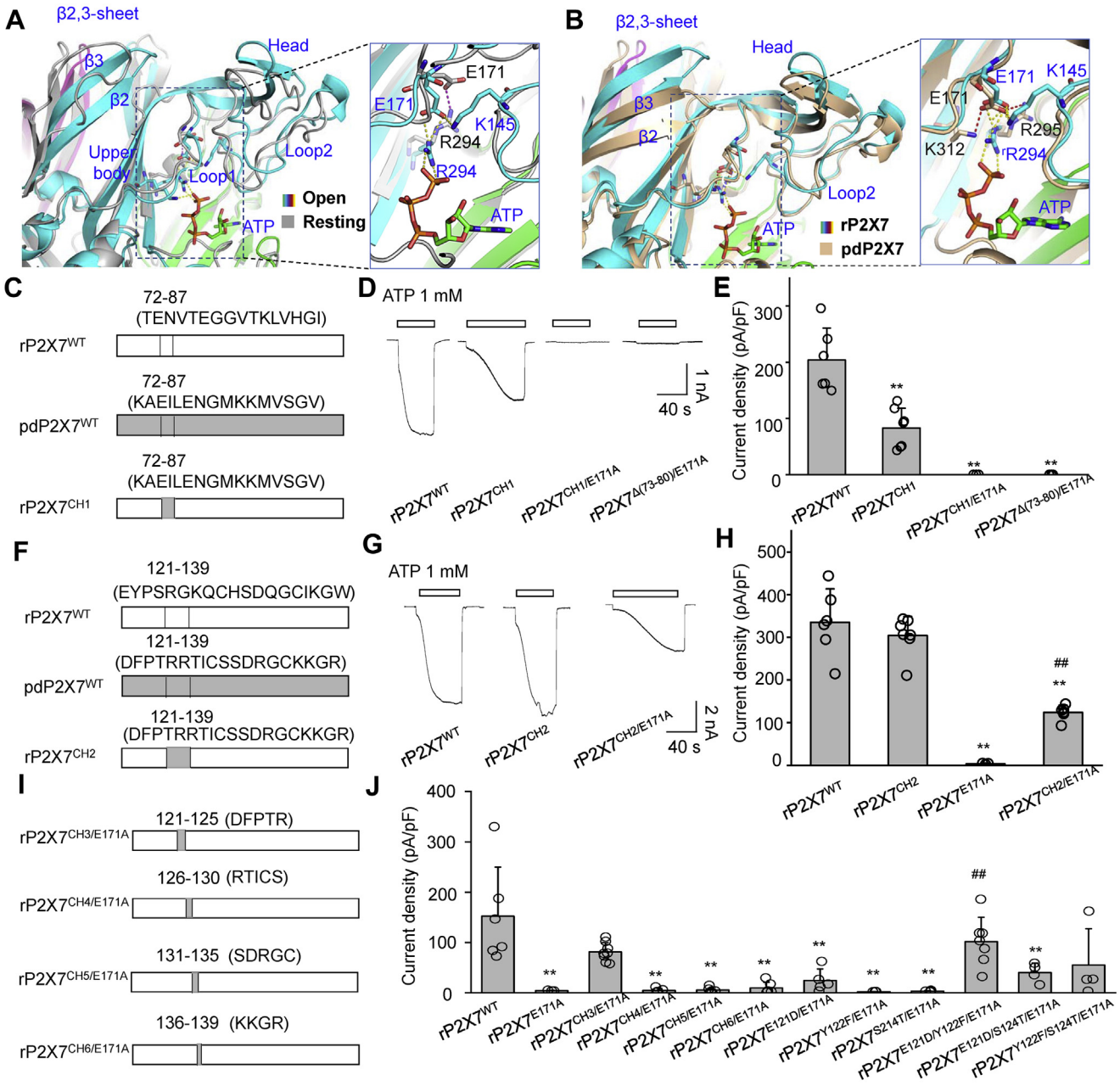

Figure 8. The longer β2,3-sheet of the P2X7 receptor negatively regulates P2X7 activation in combination with loop structures near E171. *A*, superimposed resting (*gray*) and open (*blue*) structures of rP2X7, showing magnified views of the β2,3-sheet, loop 1, loop 2, and movements toward bound ATP for E171 and R294. The yellow dashed lines show the interactions between amino acid residues. *B*, superimposed the open homology model of pdP2X7 (*blue*) and the resting structure of rP2X7 (*gold*) to show the dynamics of the β2,3-sheet, loop 1, and loop two and zoom-in view of the E171 and R294 moving closing to the bound ATP. The *yellow dotted lines* represent interactions among residues. *C*, schematic diagram of chimeric construction of rP2X7 and pdP2X7. *D–E*, representative current traces (*D*) and pooled data (*E*) for $rP2X7^{WT}$, $rP2X7^{CH1}$, $rP2X7^{CH1/E171A}$, and $rP2X7^{\Delta(73-80)/E171A}$. Data were presented as mean ± S.D. (n = 4–6), $^{**}p < 0.01$ *versus* WT, one-way ANOVA with Bonferroni post hoc test ($F(3, 17) = 33.75$, $p < 0.0001$). *F*, schematic diagram of chimera $rP2X7^{CH2}$. *G* and *H*, representative current traces (*G*) pooled data (*H*) for $rP2X7^{WT}$, $rP2X7^{CH2}$, and $rP2X7^{CH2/E171A}$. Data were presented as mean ± S.D. (n = 3–7) $^{**}p < 0.01$ *versus* WT, one-way ANOVA with Bonferroni post hoc test ($F(3, 18) = 43.94$, $p < 0.0001$). *I*, schematic diagram of chimeras. *J*, ATP current of WT and mutated rP2X7 receptors. Data were presented as mean ± S.D. (n = 3–7) $^{**}p < 0.01$ *versus* WT, ## $p < 0.01$ *versus* E171A, one-way ANOVA with Bonferroni post hoc test ($F(11, 47) = 7.455$, $p < 0.0001$).

found that the $rP2X7^{CH2/E171A}$ mutation did not completely abolish the function of rP2X7 as E171A did, with a current density of 124 ± 17 pA/pF (Fig. 8*H*), indicating that E171 and loop 2 are interdependent and can participate in the gating process together as an integrated structural element. However, replacement or deletion of the β2,3 fragment above $rP2X7^{CH2/E171A}$ still results in a nonfunctional channel. We then reduced the number of amino acids replaced at a time on top of E171A to identify important residues (Fig. 8, *I* and *J*) and found that single-amino acid substitutions, $rP2X7^{E121D/E171A}$, $rP2X7^{Y122F/E171A}$, and $rP2X7^{S214T/E171A}$, did not rescue the function of $rP2X7^{E171A}$, but the combination of two amino acids, $rP2X7^{E121D/Y122F/E171A}$, rescued it. These results suggest that loop 1… …E171… …loop 2 interactions are more complex than we expected.

To answer the question that whether or not the longer β2,3 is able to regulate the integrated structural element formed by E171 and surrounding regions during channel opening, we adopted a strategy to further extend the β2,3 structure to induce a fuller interaction of β2,3 with this integrative structural element (Fig. 9*A*). We inserted AAA, LLL, and YYY between two amino acids 78 and 79 to obtain mutations 78AAA79, 78LLL79, and 78YYY79, respectively. Their side chains become progressively larger in size and therefore have a progressively larger effect on the conformation in and around the E171/loop 2 region. Correspondingly, the currents induced by ATP were 256 ± 82, 149 ± 87, and 46.5 ± 48.2 pA/pF for 78AAA79, 78LLL79, and 78YYY79, respectively (Fig. 9, *B* and *C*). Most importantly, these insertions did not affect the surface expression of the receptor (Fig. 9, *D* and *E*). These results suggest that an appropriate β2,3 length is necessary to regulate the structural component of E171 and the surrounding regions that constitute the integrated structural element.

Then, we introduced engineered disulfide bond (cross-linking) at positions 77 and 172 to constrain the conformational change of β2,3. Interrupting the disulfide bond with dithiothreitol (DTT) treatment significantly increased the ATP-induced current of $rP2X7^{E77C/E172C}$ (ratio of $rP2X7^{E77C/E172C}$ to $rP2X7^{WT}$ = 7.03 ± 2.67 *versus* 1.05 ± 0.14, $p < 0.01$), indicating that immobilization of β2,3 resulted in impaired channel activation of P2X7 (Fig. 10, *A* and *B*).

In addition, we disrupted the structural elements formed by E171 and its surrounding region by covalent modification (Fig. 10*C*). We replaced Y122 or K174 with cysteine and introduced a bulky group (N-phenylmaleimide [NPM] of 1-phenylpyrrolidine-2,5-dione) at the position of C122 or C174 (Fig. 10*D*). The ATP-induced currents were significantly decreased after NPM pretreatment (I_{After}/I_{Before} = 0.55 ± 0.20 and 0.75 ± 0.04 *versus* 0.89 ± 0.08 for $rP2X7^{K174C}$ and $rP2X7^{Y122C}$ *versus* $rP2X7^{WT}$, Fig. 10, *E*–*G*). These results further confirm that the proper conformation of β2,3 and adjacent loop regions is essential for channel opening of the P2X7 receptor.

Discussion

Here, we provide evidence that the redundant/longer β2,3-sheet of the P2X7 receptor is important for channel function compared to other subtypes of the P2X receptor. Furthermore, amino acid E171, which is adjacent to the β2,3 region, has a different role in the activation of the P2X7 receptor than other subtypes. Further studies suggest that E171 forms a unique structural element with a region of the head loop (loop 2) involved in gating of the P2X7 receptor. β2,3 redundant fragments can be further involved in channel function by modulating this structural element.

During evolution, specific member proteins of the same family evolve into completely different structures by evolving

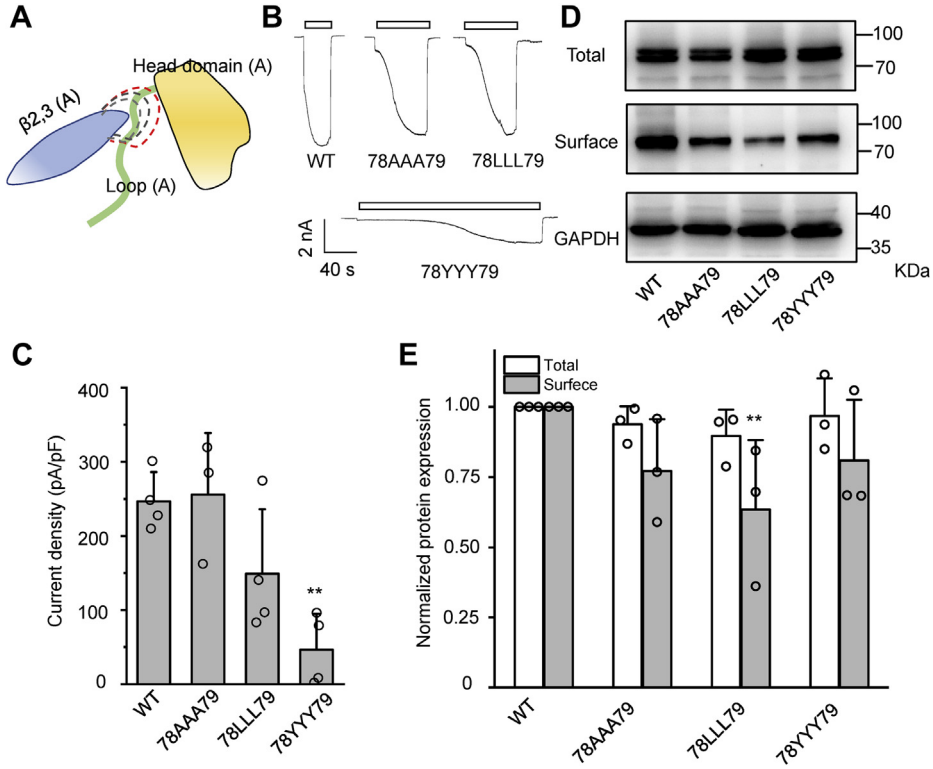

Figure 9. Alternative strategies for changing the conformation of β2,3 have a significant effect on the P2X7 receptor. *A*, schematic representation of the amino acid insertion strategy between the β2 and β3 sheets. The *blue region* is the β2,3-sheet, and the *dashed lines* represent the insertion of fragments of AAA (*light gray*), LLL (*dark gray*), and YYY (*red*) into the linker between the β2 and β3-sheets. *B* and *C*, representative current traces (*B*) and pooled data (*C*) for rP2X7-WT, 78AAA79, 78LLL79, and 78YYY79. Data are expressed as mean ± S.D. (n = 3–4). $^{**}p < 0.01$ *versus* WT, one-way ANOVA with Bonferroni post hoc test (F(3, 11) = 8.245, p = 0.0037). *D* and *E*, representative Western blotting (*D*) and pooled data (*E*) of total and surface protein expressions, and for rP2X7-WT, 78AAA79, 78LLL79, and 78YYY79. Data were presented as mean ± S.D. (n = 3). Total levels or surface levels were normalized to WT protein. $^{*}p <$ 0.05 *versus* WT, one-way ANOVA with Bonferroni post hoc test (F(3,12) = 5.292, p = 0.0148).

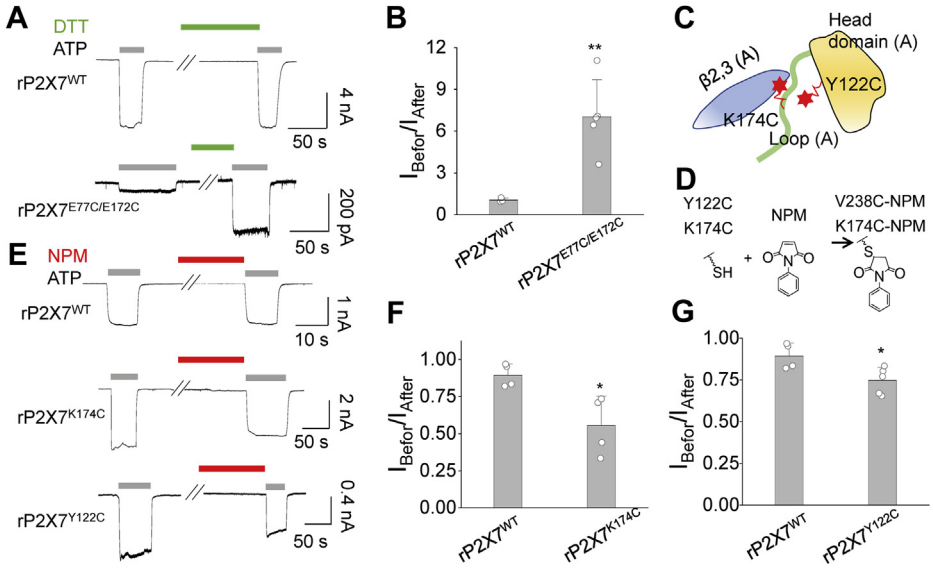

Figure 10. Perturbations of the conformation of the structural element formed by E171 and its surrounding region affect the gating of P2X7. *A* and *B*, representative current traces (*A*) and pooled date (*B*, mean ± S.D., n = 3–4) recorded from cells transfected with rP2X7$^{E77C/E172C}$ and rP2X7^{WT}. ATP (1 mM) and DTT (20 mM) were applied as the schematic indicated. **$p < 0.01$ *versus* WT. Student's *t* test. *C*, schematic representation of covalent modification at position 122 or 174. *D*, a bulky group introduced into Y122C or K174C, respectively. *E–G*, sample traces (*E*) and summarized effects of applications of NPM (1 mM) inhibited ATP-evoked currents of rP2X7^{WT}, rP2X7^{K174C} (*F*, mean ± S.D., n = 4), or rP2X7^{Y122C} (*G*, mean ± S.D., n = 4–5).*$p < 0.05$ *versus* WT. Student's *t* test.

in certain regions, thus giving that member a new regulatory mechanism and function. P2X7, studied here, may also be an example of such a process. The β2,3 region is an important part of the P2X receptor gating process (37), but the sequences constituting this region are completely different in different subtypes, and it is the longest in the P2X7 receptor. Therefore, we first deleted the redundant fragments to explore whether these redundant sequences are necessary for the channel. The results showed that the channel function was impaired after deletion (Fig. 2). There are two reasons for this impairment. *First*, the surface expression of the channel was effected upon deletion. For rP2X7, position N74 is a possible glycosylation site, and deletion of sequence resulted in the removal of the glycosylation site, which may lead to the impairment of the channel membrane expression (Fig. 3*B*). However, the region of dP2X7 has no glycosylation sites, and deletion of dP2X7 also affects the channel membrane expression, suggesting that glycosylation is not the most important reason for the reduction in surface expression caused by the deletion here (Fig. 7, *D–F*). *Second*, deletion of the redundant fragment affects not only the expression of the channel surface but also the gating process of P2X7. We found that the conformational changes of loop 1 in the P2X7 receptor near β2,3 were also unique, where mutation of E171 in loop 1 clearly affected the function of the channel, suggesting that E171 plays an important role in the gating process. However, this role is inconsistent with other P2X receptor subtypes, where mutations in E171, while affecting the ATP affinity of some subtypes, do not affect the maximum current density of other subtypes (Fig. 5). In addition, the role of β2,3 in other P2X7 species is consistent with that of E171, leading to the inference that β2,3 and E171 are interrelated (Fig. 6). By constructing chimeras with pdP2X7, i.e., β2,3 with opposite roles to rP2X7 and E171, it was found that loop 2 and E171 are jointly involved in gating regulation, while β2,3 is involved in the structural components of loop 2 and E171 regulates the gating process by influencing the movement of loop 1.

Residues 73 to 80 of β2,3 of rP2X7 may have a loose loop-like secondary structure in the resting state (the exact conformation cannot be seen due to insufficient resolution, but it should not be a stable β-sheet) but partially becomes a rigid β-sheet in the open state (30). This suggests that the β2,3 of the P2X7 receptor has changed from the resting state to the open state, whereas the secondary structure of β2,3 in the hP2X3 and zfP2X4 receptor structures does not change between the resting and open states (26, 29). β2,3 in the resting structure of pdP2X7 also exhibits a rigid β-folded structure, unlike the resting state of the rP2X7 receptor (28). Thus, in these subtypes and pdP2X7, β2,3 does not play a role in ATP activation, and the corresponding E171 sites of these P2X receptors without redundant β2,3 structures do not play an important role in channel opening. Furthermore, in the ckP2X7 receptor structures without redundant β2,3 sequences, the maximum current density of the channel is unchanged after Q159A mutations (corresponding to E171 in rP2X7), whereas the redundant β2,3 sequences of other species of P2X7 such as human, dog, guinea pig, mouse, and bovine are consistent with those of rat P2X7. In these deletion mutants, the channel current density becomes smaller, while the current density at the site corresponding to mutant E171 becomes smaller or even absent in some cases so that rP2X7 receptor β2,3 involvement in gating is associated with E171. Finally, the smaller maximum current density induced by the expansion of β2,3 by inserting YYY between 78 and 79 (Fig. 9), engineering disulfide bonds, or NPM covalent occupation (Fig. 10) also suggests an important role of β2,3 in P2X7 receptor gating.

P2X7 is one of the unique subtypes of the P2X receptor family, differing from other P2X subtypes in terms of channel characteristics and N-/C-terminals architecture (33, 36, 38). Importantly, P2X7 receptors can be used as therapeutic targets for pain, inflammation, and immune and neurological diseases (39–41). Small molecule discovery based on the unique gating mechanism of P2X7 is a viable strategy for P2X7-selective lead drug discovery (28). The function and mechanism of the unique structure of P2X7 revealed by our study can help to further understand the P2X7 receptor gating mechanism and thus provide a structural basis for drug discovery targeting P2X7 receptor subtype specificity.

Experimental procedures

Drugs, cell culture, mutagenesis, and chimeras

ATP was purchased from Sigma. Human embryonic kidney 293 cells (HEK-293) were cultured in DMEM supplemented with 10% fetal bovine serum, 1% penicillin-streptomycin, and 1% GlutaMAX at 37 °C in a humidified atmosphere of 5% CO_2 and 95% air. All mutants were constructed by the KOD-Plus-mutagenesis kit and were verified by DNA sequencing. Transfections of plasmids were performed using calcium phosphate transfection and Hieff Trans Liposomal Transfection Reagent. The plasmids pcDNA3-rP2X2, pcDNA3-rP2X4, and pcDNA3-rP2X7 were generous gifts from Drs. Alan North and Lin-Hua Jiang; the plasmid of hP2X3 was purchased from Open Biosystems; the cDNA of hP2X1 and hP2X7 were synthesized from JiKai Gene and were subcloned into the pcDNA3.1 vector; the plasmid of pdP2X7 was synthesized from Convenience Biology; the cDNA of ckP2X7 and bP2X7 were kindly gifted by Drs. Motoyuki Hattori and Osamu Nureki and were subcloned into the pcDNA3.1 vector; the cDNA of mP2X7, dP2X7, and gpP2X7 were generous gifts from Dr Ming Zhou and were subcloned into the pcDNA3.1 vector.

Electrophysiology

As we previously described (42–44), whole-cell patch clamp recordings were performed at room temperature (25 ± 2 °C), using an Axopatch 200B under the voltage clamp. Membrane currents were filtered at 2 kHz. All currents were sampled and analyzed using a Digidata 1550B interface and a computer running the Clampex and Clampfit 10.0 software (Molecular Devices). The extracellular solution containing (in millimolar, mM) 150 NaCl, 5 KCl, 10 glucose, 10 Hepes, 2 $CaCl_2$ and 1 $MgCl_2$, and the pH was adjusted to 7.35 to 7.4. The pipette solutions contained (mM) 120 KCl, 30 NaCl, 0.5 $CaCl_2$, 1 $MgCl_2$, 10 Hepes, and 5 EGTA, and the pH was adjusted to 7.2. The membrane potential was held at -60 mV. ATP was dissolved in external solutions and applied with the Y-tube. As we previously described (45), nystatin-perforated patch clamp was carried out to reduce the dialysis of intracellular constituents and avoid the desensitization of P2X receptors. Nystatin in high-potassium pipette solutions contained (mM) 75 K_2SO_4, 55 KCl, 5 $MgSO_4$ and 10 Hepes, pH 7.2. ATP-gated currents were recorded after regular 10- to 15-s ATP applications every 6 to 8 min.

Western blotting

Western blotting and surface biotinylation were performed according to our previous description (37, 46, 47). HEK-293 cells expressing rP2X7 or its mutants were washed in chilled $PBS^{+/+}$ and then incubated with sulfo-NHS-LC-biotin. The reaction was terminated by incubating the cells with glycine (20 mM) in PBS. The cells were then collected and lysed with radio immunoprecipitation assay lysis buffers. With centrifugation, 20% the volume of the supernatant was diluted with SDS loading buffer as the total protein fraction. The remaining lysate was incubated with NeutrAvidin agarose resin at 4 °C in 4 to 5 h, and then the resin was washed five times with chilled PBS and diluted with SDS loading buffer, used as surface proteins fractions. The protein samples were separated by SDS-PAGE and transferred to a polyvinylidene difluoride (PVDF) membrane. The PVDF membrane was blocked with 5% milk at room temperature for 1 to 2 h and then incubated overnight at 4 °C with anti-P2X7 (1:200, Calbiochem) or anti-GAPDH (1:3000, Sungene Biotech) antibodies dissolved in 5% milk. The PVDF membrane was washed 4 to 5 times with Tris Buffered Saline with Tween 20. Appropriate horseradish peroxidase (HRP)-conjugated secondary antibodies for anti-P2X7 (25 °C, 1 h, 1:3000, goat-rabbit IgG (H+L)HRP) or GAPDH (25 °C, 1 h, 1:3000, goat-mouse IgG (H+L)-HRP). Finally, the blots were visualized by exposure with automated chemiluminescence-fluorescence image analysis systems (Tanon 5200, Multi) for 1 to 3 min in ECL solution (Thermo). Analysis of protein expression was repeated by at least three independent experiments.

Data analysis

The results were expressed as the means ± SD. Statistical comparisons were made using Bonferroni *post hoc* test (ANOVA) or the Student's *t* test. $^{*}p < 0.05$ and $^{**/\#\#}p < 0.01$ were considered significant. Concentration–response relationships for ATP activation of WT or mutants were obtained by measuring currents in response to different concentrations of ATP. The data were fitted to the equation as $I/I_{max} = 1/[1 + (EC_{50}/[ATP])^{n}]$, where I is the normalized current at a given concentration of ATP, I_{max} is the maximum normalized current, EC_{50} is the concentration of ATP yielding one half of maximal currents, and n is the Hill coefficient.

Data availability

All data are contained within the manuscript.

Author contributions—X-. F. M., T-. T. W., W-. H. W., L. G., X-. H. L., Y-. T. L., Y-. Z. F., X-. N. Y., Y. Y., Y. T., and J. W. methodology; X-. F. M., T-. T. W., W-. H. W., O. N., Y. Y., Y. T., and J. W. validation; X-. F. M., T. T. W., Y. Y., and J. W. formal analysis; X-. F. M., T-. T. W., L. G., C-. R. G., X-. H. L., Y-. T. L., Y. Z. F., X-. N. Y., M. H., M. X. Z., Y. T., and J. W. investigation; X-. F. M., T-. T. W., L. G., C-. R. G., X-. H. L., Y-. T. L., Y. Z-. F., Y. Y., and J. W. data curation; X-. F. M., Y. Y., and J. W. visualization; X-. F. M. writing-original draft; W-. H. W., X-. N. Y., Y. Y., Y. T., and J. W. funding acquisition; M. H., O. N., Y. Y., Y. T., and J. W. resources; M. X. Z., Y. Y., and J. W, writing-

review and editing; Y. Y. conceptualization; Y. Y. and J. W. supervision; Y. Y., Y. T., and J. W. project administration.

Funding and additional information—This study was supported with funds from the Natural Science Foundation of Jiangsu Province (BK20202002 to Y. Y.), National Natural Science Foundation of China with grant numbers 32000869 (J. W.), 31971042 (Y. T.), 81603409 (Y. -Z. F.), 31900808 (X-. N. Y.), 81902480 (W-. H. W.), and 31971146 (Y. Y.), Innovation and Entrepreneurship Talent Program of Jiangsu Province (Y. Y. and J. W.), State Key Laboratory of Utilization of Woody Oil Resource with grant number 2019XK2002 (Y. Y.), Hunan Provincial Natural Science Foundation of China (2018JJ1012 to Y. T.), Hunan "Huxiang" High-level Talent Program (2021 to Y. Y) and "Xing Yao" Leading Scholars of China Pharmaceutical University (2021) (Y. Y). This work was also supported by the Innovative Research Team of High-level Local Universities in Shanghai and a key laboratory program of the Education Commission of Shanghai Municipality (ZDSYS14005) and by the Open Research Fund of State Key Laboratory of Genetic Engineering, Fudan University (No. SKLGE-2105).

Conflict of interest—The authors declare that they have no conflicts of interest with the contents of this article.

Abbreviations—The abbreviations used are: HRP, horseradish peroxidase.

References

1. Brake, A. J., Wagenbach, M. J., and Julius, D. (1994) New structural motif for ligand-gated ion channels defined by an ionotropic ATP receptor. *Nature* **371**, 519–523
2. Valera, S., Hussy, N., Evans, R. J., Adami, N., North, R. A., Surprenant, A., *et al.* (1994) A new class of ligand-gated ion channel defined by P2x receptor for extracellular ATP. *Nature* **371**, 516–519
3. Lewis, C., Neidhart, S., Holy, C., North, R. A., Buell, G., and Surprenant, A. (1995) Coexpression of P2X2 and P2X3 receptor subunits can account for ATP-gated currents in sensory neurons. *Nature* **377**, 432–435
4. Collo, G., North, R. A., Kawashima, E., Merlo-Pich, E., Neidhart, S., Surprenant, A., *et al.* (1996) Cloning OF P2X5 and P2X6 receptors and the distribution and properties of an extended family of ATP-gated ion channels. *J. Neurosci.* **16**, 2495–2507
5. Soto, F., Garcia-Guzman, M., Gomez-Hernandez, J. M., Hollmann, M., Karschin, C., and Stühmer, W. (1996) P2X4: an ATP-activated ionotropic receptor cloned from rat brain. *Proc. Natl. Acad. Sci. U. S. A.* **93**, 3684–3688
6. Chen, C. C., Akopian, A. N., Sivilotti, L., Colquhoun, D., Burnstock, G., and Wood, J. N. (1995) A P2X purinoceptor expressed by a subset of sensory neurons. *Nature* **377**, 428–431
7. Surprenant, A., Rassendren, F., Kawashima, E., North, R. A., and Buell, G. (1996) The cytolytic P2Z receptor for extracellular ATP identified as a P2X receptor (P2X7). *Science (New York, N.Y.)* **272**, 735–738
8. North, R. A., and Surprenant, A. (2000) Pharmacology of cloned P2X receptors. *Annu. Rev. Pharmacol. Toxicol.* **40**, 563–580
9. Jarvis, M. F., and Khakh, B. S. (2009) ATP-gated P2X cation-channels. *Neuropharmacology* **56**, 208–215
10. Koshimizu, T., Koshimizu, M., and Stojilkovic, S. S. (1999) Contributions of the C-terminal domain to the control of P2X receptor desensitization. *J. Biol. Chem.* **274**, 37651–37657
11. Nuttle, L. C., and Dubyak, G. R. (1994) Differential activation of cation channels and non-selective pores by macrophage P2z purinergic receptors expressed in Xenopus oocytes. *J. Biol. Chem.* **269**, 13988–13996
12. Steinberg, T. H., Newman, A. S., Swanson, J. A., and Silverstein, S. C. (1987) ATP^{4-} permeabilizes the plasma membrane of mouse macrophages to fluorescent dyes. *J. Biol. Chem.* **262**, 8884–8888
13. Di Virgilio, F., Dal Ben, D., Sarti, A. C., Giuliani, A. L., and Falzoni, S. (2017) The P2X7 receptor in infection and inflammation. *Immunity* **47**, 15–31
14. Borges da Silva, H., Beura, L. K., Wang, H., Hanse, E. A., Gore, R., Scott, M. C., *et al.* (2018) The purinergic receptor P2RX7 directs metabolic fitness of long-lived memory CD8(+) T cells. *Nature* **559**, 264–268
15. Karmakar, M., Katsnelson, M. A., Dubyak, G. R., and Pearlman, E. (2016) Neutrophil P2X7 receptors mediate NLRP3 inflammasome-dependent IL-1β secretion in response to ATP. *Nat. Commun.* **7**, 10555
16. Amores-Iniesta, J., Barberà-Cremades, M., Martínez, C. M., Pons, J. A., Revilla-Nuin, B., Martínez-Alarcón, L., *et al.* (2017) Extracellular ATP activates the NLRP3 inflammasome and is an early danger signal of skin allograft rejection. *Cell Rep.* **21**, 3414–3426
17. Chen, X., Hu, J., Jiang, L., Xu, S., Zheng, B., Wang, C., *et al.* (2014) Brilliant Blue G improves cognition in an animal model of Alzheimer's disease and inhibits amyloid-β-induced loss of filopodia and dendrite spines in hippocampal neurons. *Neuroscience* **279**, 94–101
18. Díaz-Hernández, M., Díez-Zaera, M., Sánchez-Nogueiro, J., Gómez-Villafuertes, R., Canals, J. M., Alberch, J., *et al.* (2009) Altered P2X7-receptor level and function in mouse models of Huntington's disease and therapeutic efficacy of antagonist administration. *FASEB J.* **23**, 1893–1906
19. Amadio, S., Parisi, C., Piras, E., Fabbrizio, P., Apolloni, S., Montilli, C., *et al.* (2017) Modulation of P2X7 receptor during inflammation in multiple sclerosis. *Front. Immunol.* **8**, 1529
20. Adinolfi, E., Raffaghello, L., Giuliani, A. L., Cavazzini, L., Capece, M., Chiozzi, P., *et al.* (2012) Expression of P2X7 receptor increases *in vivo* tumor growth. *Cancer Res.* **72**, 2957–2969
21. Sorge, R. E., Trang, T., Dorfman, R., Smith, S. B., Beggs, S., Ritchie, J., *et al.* (2012) Genetically determined P2X7 receptor pore formation regulates variability in chronic pain sensitivity. *Nat. Med.* **18**, 595–599
22. Letavic, M. A., Savall, B. M., Allison, B. D., Aluisio, L., Andres, J. I., De Angelis, M., *et al.* (2017) 4-Methyl-6,7-dihydro-4H-triazolo[4,5-c]pyridine-Based P2X7 receptor antagonists: optimization of pharmacokinetic properties leading to the identification of a clinical candidate. *J. Med. Chem.* **60**, 4559–4572
23. Calzaferri, F., Ruiz-Ruiz, C., de Diego, A. M. G., de Pascual, R., Méndez-López, I., Cano-Abad, M. F., *et al.* (2020) The purinergic P2X7 receptor as a potential drug target to combat neuroinflammation in neurodegenerative diseases. *Med. Res. Rev.* **40**, 2427–2465
24. Sperlágh, B., and Illes, P. (2014) P2X7 receptor: an emerging target in central nervous system diseases. *Trends Pharmacol. Sci.* **35**, 537–547
25. Kawate, T., Michel, J. C., Birdsong, W. T., and Gouaux, E. (2009) Crystal structure of the ATP-gated P2X4 ion channel in the closed state. *Nature* **460**, 592–598
26. Hattori, M., and Gouaux, E. (2012) Molecular mechanism of ATP binding and ion channel activation in P2X receptors. *Nature* **485**, 207–212
27. Kasuya, G., Fujiwara, Y., Takemoto, M., Dohmae, N., Nakada-Nakura, Y., Ishitani, R., *et al.* (2016) Structural insights into divalent cation modulations of ATP-gated P2X receptor channels. *Cell Rep.* **14**, 932–944
28. Karasawa, A., and Kawate, T. (2016) Structural basis for subtype-specific inhibition of the P2X7 receptor. *Elife* **5**, e22153
29. Mansoor, S. E., Lu, W., Oosterheert, W., Shekhar, M., Tajkhorshid, E., and Gouaux, E. (2016) X-ray structures define human P2X(3) receptor gating cycle and antagonist action. *Nature* **538**, 66–71
30. McCarthy, A. E., Yoshioka, C., and Mansoor, S. E. (2019) Full-length P2X7 structures reveal how palmitoylation prevents channel desensitization. *Cell* **179**, 659–670.e613
31. Kasuya, G., Yamaura, T., Ma, X.-B., Nakamura, R., Takemoto, M., Nagumo, H., *et al.* (2017) Structural insights into the competitive inhibition of the ATP-gated P2X receptor channel. *Nat. Commun.* **8**, 876
32. Wang, J., Wang, Y., Cui, W. W., Huang, Y., Yang, Y., Liu, Y., *et al.* (2018) Druggable negative allosteric site of P2X3 receptors. *Proc. Natl. Acad. Sci. U. S. A.* **115**, 4939–4944
33. Costa-Junior, H. M., Sarmento Vieira, F., and Coutinho-Silva, R. (2011) C terminus of the P2X7 receptor: treasure hunting. *Purinergic Signal.* **7**, 7–19
34. Allsopp, R. C., and Evans, R. J. (2015) Contribution of the juxta-transmembrane intracellular regions to the time course and permeation of ATP-gated P2X7 receptor ion channels. *J. Biol. Chem.* **290**, 14556–14566

35. Liang, X., Samways, D. S., Wolf, K., Bowles, E. A., Richards, J. P., Bruno, J., *et al.* (2015) Quantifying Ca^{2+} current and permeability in ATP-gated P2X7 receptors. *J. Biol. Chem.* **290**, 7930–7942
36. Amstrup, J., and Novak, I. (2003) P2X7 receptor activates extracellular signal-regulated kinases ERK1 and ERK2 independently of Ca2+ influx. *Biochem. J.* **374**, 51–61
37. Zhao, W. S., Sun, M. Y., Sun, L. F., Liu, Y., Yang, Y., Huang, L. D., *et al.* (2016) A highly conserved salt bridge stabilizes the kinked conformation of beta2,3-sheet essential for channel function of P2X4 receptors. *J. Biol. Chem.* **291**, 7990–8003
38. Yan, Z., Li, S., Liang, Z., Tomić, M., and Stojilkovic, S. S. (2008) The P2X7 receptor channel pore dilates under physiological ion conditions. *J. Gen. Physiol.* **132**, 563–573
39. Bhattacharya, A. (2018) Recent advances in CNS P2X7 physiology and pharmacology: focus on neuropsychiatric disorders. *Front. Pharmacol.* **9**, 30
40. Beamer, E., Fischer, W., and Engel, T. (2017) The ATP-gated P2X7 receptor as a target for the treatment of drug-resistant epilepsy. *Front. Neurosci.* **11**, 21
41. Gelin, C. F., Bhattacharya, A., and Letavic, M. A. (2020) P2X7 receptor antagonists for the treatment of systemic inflammatory disorders. *Prog. Med. Chem.* **59**, 63–99
42. Zhao, W. S., Wang, J., Ma, X. J., Yang, Y., Liu, Y., Huang, L. D., *et al.* (2014) Relative motions between left flipper and dorsal fin domains favour P2X4 receptor activation. *Nat. Commun.* **5**, 4189
43. Sun, L. F., Liu, Y., Wang, J., Huang, L. D., Yang, Y., Cheng, X. Y., *et al.* (2019) Altered allostery of the left flipper domain underlies the weak ATP response of rat P2X5 receptors. *J. Biol. Chem.* **294**, 19589–19603
44. Li, B., Wang, J., Cheng, X., Liu, Y., Yang, Y., Yang, X., *et al.* (2018) Molecular mechanism underlying the subtype-selectivity of competitive inhibitor NF110 and its distinct potencies in human and rat P2X3 receptors. *Sci. Bull.* **63**, 1616–1625
45. Chen, P. F., Ma, X. F., Sun, L. F., Tian, Y., Fan, Y. Z., Li, P., *et al.* (2021) A conserved residue in the P2X4 receptor has a nonconserved function in ATP recognition. *J. Biol. Chem.* **296**, 100655
46. Yang, Y., Yu, Y., Cheng, J., Liu, Y., Liu, D. S., Wang, J., *et al.* (2012) Highly conserved salt bridge stabilizes rigid signal patch at extracellular loop critical for surface expression of acid-sensing ion channels. *J. Biol. Chem.* **287**, 14443–14455
47. Wang, J., Sun, L. F., Cui, W. W., Zhao, W. S., Ma, X. F., Li, B., *et al.* (2017) Intersubunit physical couplings fostered by the left flipper domain facilitate channel opening of P2X4 receptors. *J. Biol. Chem.* **292**, 7619–7635